Geosci. Model Dev. Discuss., 7, 6845–6891, 2014
www.geosci-model-dev-discuss.net/7/6845/2014/
doi:10.5194/gmdd-7-6845-2014

Geoscientific Model Development Discussions

A test of an optimal stomatal conductance scheme within the CABLE Land Surface Model

M. G. De Kauwe[1], J. Kala[2], Y.-S. Lin[1], A. J. Pitman[2], B. E. Medlyn[1], R. A. Duursma[3], G. Abramowitz[2], Y.-P. Wang[4], and D. G. Miralles[5]

[1]Macquarie University, Sydney, Australia
[2]Australian Research Council Centre of Excellence for Climate Systems Science and Climate Change Research Centre, Sydney, Australia
[3]Hawkesbury Institute for the Environment, University of Western Sydney, Sydney, Australia
[4]CSIRO Marine and Atmospheric Research and Centre for Australian Weather and Climate Research, Private Bag #1, Aspendale, Victoria 3195, Australia
[5]School of Geographical Sciences, University of Bristol, Bristol, England

Received: 29 September 2014 – Accepted: 4 October 2014 – Published: 15 October 2014

Correspondence to: M. G. De Kauwe (mdekauwe@gmail.com)

Published by Copernicus Publications on behalf of the European Geosciences Union.

Abstract

Stomatal conductance (g_s) affects the fluxes of carbon, energy and water between the vegetated land surface and the atmosphere. We test an implementation of an optimal stomatal conductance model within the Community Atmosphere Biosphere Land Exchange (CABLE) land surface model (LSM). In common with many LSMs, CABLE does not differentiate between g_s model parameters in relation to plant functional type (PFT), but instead only in relation to photosynthetic pathway. We therefore constrained the key model parameter "g_1" which represents a plants water use strategy by PFT based on a global synthesis of stomatal behaviour. As proof of concept, we also demonstrate that the g_1 parameter can be estimated using two long-term average (1960–1990) bioclimatic variables: (i) temperature and (ii) an indirect estimate of annual plant water availability. The new stomatal models in conjunction with PFT parameterisations resulted in a large reduction in annual fluxes of transpiration (~ 30 % compared to the standard CABLE simulations) across evergreen needleleaf, tundra and C4 grass regions. Differences in other regions of the globe were typically small. Model performance when compared to upscaled data products was not degraded, though the new stomatal conductance scheme did not noticeably change existing model-data biases. We conclude that optimisation theory can yield a simple and tractable approach to predicting stomatal conductance in LSMs.

1 Introduction

Land surface models (LSMs) provide the lower boundary conditions in global climate and weather prediction models. A key role for LSMs is to calculate net radiation available at the surface and its partitioning between sensible and latent heat fluxes (Pitman, 2003). To achieve this, LSMs calculate latent heat exchange between the soil, vegetation and the atmosphere. This latent heat exchange involves a transfer of water vapour to the atmosphere; for vegetated surfaces this transfer (i.e. transpiration) occurs mostly

through the stomatal cells on the leaves as they open to uptake CO_2 for photosynthesis. The stomata thus provide the principal control mechanism over the exchange of water and the associated flux of carbon dioxide (CO_2) between the leaf and the atmosphere. Stomatal conductance (g_s) plays a significant role in global carbon, energy and water cycles (Henderson-Sellers et al., 1995; Pollard and Thompson, 1995; Cruz et al., 2010), in determining regional temperatures (Cruz et al., 2010) and as a potential feedback to climate change (Sellers et al., 1996; Gedney et al., 2006; Betts et al., 2007; Cao et al., 2010).

Within both ecosystem and land surface models, a common approach to representing g_s has been to use empirical models (Jarvis, 1976; Ball et al., 1987; Leuning, 1995; see Damour et al., 2010, for a review). In a recent inter-comparison study, 10 of the 11 ecosystem models considered applied some form of the "Ball–Berry–Leuning" approach (De Kauwe et al., 2013a). The empirical nature of these models means that we cannot attach any theoretical significance to differences in model parameters, be it across datasets or among species. As a consequence, models which use these schemes typically either assume the model parameters do not vary between plant functional type (PFT) but only photosynthetic pathway (Krinner et al., 2005; Oleson et al., 2013), or tune the parameters to match a specific experiment where necessary. Whilst more mechanistic g_s models have been proposed (e.g. Buckley et al., 2003; Wang et al., 2012), they have not been widely tested due to their relative complexity and the need to obtain additional model parameters, for which we have no or limited observational data across a variety of PFTs.

An alternative approach, which builds on the original work by Cowan and Farquhar (1977) and Cowan (1982), shows that stomatal conductance can be modelled using an optimisation framework (Hari et al., 1986; Lloyd, 1991; Arneth et al., 2002; Katul et al., 2009; Schymanski et al., 2009; Medlyn et al., 2011). This approach hypothesises that stomata behave optimally, by maximising carbon gain (photosynthesis, A) whilst minimising water loss (transpiration, E) over some period of time ($t_2 - t_1$), represented

by maximising:

$$\int_{t_1}^{t_2} (A(t) - \lambda E(t)) \mathrm{d}t \quad (1)$$

where λ ($\mathrm{mol}^{-1}\,\mathrm{C}\,\mathrm{mol}^{-1}\,\mathrm{H_2O}$) is the marginal carbon cost of water use. It is possible to implement a numerical solution of this optimisation problem into an LSM (Bonan et al., 2014) but the resulting model is highly computationally intensive.

Medlyn et al. (2011) recently proposed a tractable model that analytically solves the optimisation problem. This model has great potential because it combines a simple functional form, similar to current empirical approaches, with a theoretical basis. Biological meaning can be attached to the parameters, which can then be hypothesised to vary with climate and plant water use strategy (Medlyn et al., 2011; Héroult et al., 2013; Lin et al. 2014). In addition, the behaviour of this model has been widely tested at the leaf scale and it has been shown to perform at least as well, if not better than, the more widespread empirical approaches currently used (Medlyn et al., 2011, 2013; De Kauwe et al., 2013a; Héroult et al., 2013).

We present an implementation of the Medlyn et al. (2011) optimal stomatal conductance model within the Community Atmosphere Biosphere Land Exchange (CABLE) LSM (Wang et al., 2011). CABLE is the LSM used within the Australian Community Climate Earth System Simulator (ACCESS, see http://www.accessimulator.org.au; Kowalczyk et al., 2013), a fully coupled earth system model used as part of the Coupled Model Intercomparison Project (CMIP-5) which in turn informed much of the climate projection research underpinning the 5th assessment report of the Intergovernmental Panel on Climate Change. CABLE currently implements an empirical representation of g_s following Leuning et al. (1995). The implementation assumes that all PFTs can be adequately described by three parameters, two of which vary with photosynthetic pathway, rather than any physiological properties of the PFT. In contrast, here we seek to constrain the new Medlyn model implementation with data derived from a recent global

synthesis of stomatal behaviour (Lin et al. 2014). We first test the implementation of the new g_s scheme at a series of flux tower sites and then undertake a series of offline simulations to examine the model's behaviour at the global scale.

2 Methods

2.1 Model description

The CABLE LSM has been used extensively for both coupled (Cruz et al., 2010; Pitman et al., 2011; Mao et al., 2011; Lorenz et al., 2014) and offline simulations (Abramowitz et al., 2008; Wang et al., 2011; Kala et al., 2014) at a range of spatial scales. CABLE represents the canopy using a single layer, two-leaf canopy model separated into sunlit and shaded leaves (Leuning et al., 1995; Wang and Leuning, 1998), with aerodynamic properties simulated as a function of canopy height and leaf area index (LAI) (Raupach, 1994, 1997). The Richards' equation for soil water and heat conduction for soil temperature are numerically integrated using a six discrete soil layers, and up to three layers of snow can accumulate on the soil surface. A more complete description can be found in Kowalczyk et al. (2006) and Wang et al. (2011). The version of CABLE used in this study, CABLEv2.0.1, has been evaluated by Lorenz et al. (2014) when coupled to ACCESS and shown to have excessive evaporation, leading to unrealistically small diurnal temperature ranges. Here we focus on the parameterisation of stomatal conductance. The source code can be accessed after registration at https://trac.nci.org.au/trac/cable.

2.2 Stomatal model and parameterisation

In CABLE model, g_s is modelled following Leuning et al. (1995):

$$g_s = g_0 + \frac{a_1 \beta A}{(C_s - \Gamma)\left(1 + \frac{D}{D_0}\right)} \quad (2)$$

where A is the gross assimilation rate (μmol m^{-2} s^{-1}), g_s is the stomatal conductance (mol m^{-2} s^{-1}), C_s (μmol mol^{-1}) and D (kPa) are the CO_2 concentration and the vapour pressure deficit at the leaf surface, respectively, Γ (μmol mol^{-1}) is the CO_2 compensation point of photosynthesis, and g_0 (mol m^{-2} s^{-1}), D_0 (kPa) and a_1 are fitted constants representing the residual stomatal conductance as the assimilation rate reaches zero, the sensitivity of stomatal conductance to D and the slope of the sensitivity of stomatal conductance to assimilation, respectively. In CABLE, the fitted parameters g_0 and a_1 vary with photosynthetic pathway (C3 vs. C4) but not PFT, and D_0 is fixed for all PFTs. g_0 is scaled from the leaf to the canopy by accounting for LAI, following Wang and Leuning (1998). β represents an empirical soil moisture stress factor. For these simulations we used the standard CABLE implementation throughout:

$$\beta = \frac{\theta - \theta_w}{\theta_{fc} - \theta_w}; \beta[0,1] \quad (3)$$

where θ is the mean volumetric soil moisture content (m^3 m^{-3}) in the root zone, θ_w is the wilting point (m^3 m^{-3}) and θ_{fc} is the field capacity (m^3 m^{-3}).

In this study we replaced Eq. (2) with the g_s model of Medlyn et al. (2011):

$$g_s = g_0 + 1.6\left(1 + \frac{g_1 \beta}{\sqrt{D}}\right)\frac{A}{C_s} \quad (4)$$

where g_1 ($kPa^{0.5}$) is a fitted parameter representing the sensitivity of the conductance to the assimilation rate. In this formulation of the g_s model, the g_1 parameter has a theoretical meaning and is proportional to:

$$g_1 \propto \sqrt{\frac{\Gamma^*}{\lambda}} \quad (5)$$

where λ is defined by Eq. (1) and Γ^* (μmol mol^{-1}) is the CO_2 compensation point in the absence of mitochondrial respiration. As a result, g_1 is inversely related to the

marginal carbon cost of water, λ, and is predicted to decrease with drought severity, but to increase with growth temperature (Lin et al. 2014).

Figure 1 shows the stomatal sensitivity to increasing D predicted by the two models. In this comparison, the Medlyn model has been calibrated using least squares against g_s values predicted by the Leuning model, where D varies between 0.05 and 3 kPa. The Leuning model was parameterised in the same way as the CABLE model, for C3 species: $g_0 = 0.01\,\mathrm{mol\,m^{-2}\,s^{-1}}$, $a_1 = 9.0$, $D_0 = 1.5\,\mathrm{kPa}$ and for C4 plants: $g_0 = 0.04\,\mathrm{mol\,m^{-2}\,s^{-1}}$, $a_1 = 4.0$, $D_0 = 1.5\,\mathrm{kPa}$. The calibrated parameters for the Medlyn model were $g_1 = 3.37\,\mathrm{kPa}^{0.5}$ and $g_1 = 1.10\,\mathrm{kPa}^{0.5}$ for C3 and C4 species, respectively. Over low to moderate D ranges (< 1.5 kPa), the Medlyn model can be seen to decline more steeply than the Leuning model. There is then a clear crossover point between the two models, where the Leuning model predicts g_s continues to decline with increasing D, whereas the Medlyn model predicts that g_s is less sensitive to increasing D. In the Leuning model the different transition points in the C3 and C4 simulations result from the species parameterisation of D_0. We use this calibration of the Medlyn model (MED-L) to the Leuning model (LEU) throughout this manuscript, in order to distinguish structural difference between the models from differences resulting from model parameterisation (MED-P).

Lin et al. (2014) compiled a global synthesis of stomatal behaviour within the framework of the Medlyn model from 314 species across 56 field studies, which covered a wide range of biomes from Arctic tundra, boreal and temperate forests to tropical rainforest. We estimated the parameter values for g_1 for each of CABLE's 10 vegetation PFTs by fitting Eq. (4) to the leaf gas exchange dataset of Lin et al. (2014) with a non-linear mixed-effects model. The model was fit to data for each PFT separately, using species as a random effect on the g_1 parameter (to account for correlation of observations within species groups). For all mixed-effects models, we used the *lme4* package in R version 3.1.0 (R Core Development Team, 2014).

Stomatal optimisation theory would predict that g_s would be zero when photosynthesis was also zero, and thus, there would be no g_0 parameter in the model. However,

the g_0 parameter was retained by Medlyn et al. (2011) in order to ensure the correct behaviour of intercellular CO_2 concentration (C_i), as A approaches zero. The parameter g_0 represents the stomatal conductance when photosynthesis is zero, which may occur when light or temperature are low or when VPD is high. In most cases this value is small or negligible. This parameter can be estimated independently of g_1 if measurements of stomatal conductance under low-A conditions are available (Leuning, 1995). However, without such data it is inadvisable to estimate g_0, as high values of g_0 then tend to indicate lack of fit of the model rather than the true value of g_0. Values of g_1 will be anti-correlated with values of g_0, rendering it impossible to compare values of g_1 across datasets. The dataset of Lin et al. (2014) did not include appropriate measurements to estimate g_0 independently of g_1 so we set g_0 equal to zero for this study.

Additionally, the dataset compiled by Lin et al. (2014) did not have measurements that covered deciduous needleleaf PFTs. As Lin et al. (2014) hypothesised that the high marginal cost of water in evergreen conifers is a consequence of the lack of vessels for water transport in conifer stemwood, we assumed that the marginal cost of water for deciduous needleleaf trees would be similar to that of evergreens. Therefore, for the deciduous needleleaf PFT we use the same parameters as the evergreen needleleaf PFT.

Lin et al. (2014) also demonstrated a significant relationship ($r^2 = 0.43$) between g_1 and two long-term average (1960–1990) bioclimatic variables: temperature and a moisture index representing an indirect estimate of plant water availability. First, they estimated g_1 for each species separately using non-linear regression, and then they fit Eq. (4) to these individual estimates of g_1.

$$\log(g_1) = a + b \times \mathrm{MI} + c \times \overline{T} + d \times \mathrm{MI} \times \overline{T} \quad (6)$$

where a, b, c, and d are model coefficients, $\overline{T}$ is the mean temperature during the period when temperature is above 0 °C, MI is a moisture index calculated as the ratio of mean precipitation to the equilibrium evapotranspiration (as described in Gallego-Sala et al., 2010). Equation (6) was fit using a linear mixed-effects model, where PFT

was used as random intercept, because we assume g_1 observations were independent observations for a given PFT.

We derived global MI and $\overline{T}$ values from Climate Research Unit (CRU) CL1.0 climatology data set (1961–1990), interpolating the 0.5° data to 1.0° to match the resolution of the global offline forcing used, using a nearest neighbour approach. We masked land surface areas in the CRU data which did not correspond to one of CABLE 10 PFTs. In addition, we also masked pixels where there are no MI and $\overline{T}$ values (40 pixels). To directly evaluate the differences in g_1 responses to the two climatic variables amongst PFTs, we modified Eq. (6):

$$\log(g_1) = a + b \times \mathrm{MI} + c \times \overline{T} + d \times \mathrm{MI} \times \overline{T} + e \times \mathrm{PFT} \quad (7)$$

where a, b, c, d and e are model coefficients (Table, 2). We fitted Eq. (6) to the individual estimates of g_1 by species (see above), but this time with a linear regression model (because PFT here is assumed to be a fixed effect). We then used the estimated model coefficients to predict g_1 values (MED-C) based on the MI and $\overline{T}$ values for each pixel. Standard errors of the prediction were calculated with standard methods for linear regression. Finally, we masked pixels where MI or $\overline{T}$ values are outside the range (MI > 3.26; $\overline{T}$ > 29.7 °C) covered by the g_s synthesis database (126 pixels) to avoid extrapolation of the model. As proof of concept, here we also test the impact of parameterising CABLE with the g_1 parameter predicted from these climate indices (MED-C).

Global maps of the predicted g_1 parameter (Fig. 2a) show a clear latitudinal gradient. Lower values of g_1, which represent a more conservative water use strategy, are found across mid-latitudes (20–60° N) and higher values of g_1 are located towards more humid regions. Figure 2b shows the within PFT variation of g_1, driven by the assumed relationships between g_1 and the climate indices (temperature and aridity). This is particularly evident across the tropics, where the impact of temperature results in gradients of g_1 values which are not evident in Fig. 2a. Parameter uncertainty maps (±2 standard errors) of the g_1 parameter are shown in Fig. A1. These maps indicate

considerable uncertainty in deriving the g_1 parameter as a function of these climate relationships (Fig. A1c and d), particularly for C3 grasses (mean (μ) range = 1.42–8.8) and C3 crops (μ range = 3.99–8.89) PFTs.

2.3 Model simulations

In addition to the control simulation using the Leuning model (LEU), we carried out three further model simulations; testing the impact of model structure (MED-L), parameterisation synthesised from experimental data (MED-P) and parameterisation based on a set of climatic indices (temperature and aridity) (MED-C) (Table 3). Simulations were first carried out at 6 flux sites selected from the FLUXNET network (http://www.fluxdata.org/). These covered a range of CABLE PFTs: (i) deciduous broadleaf forest, (ii) evergreen broadleaf forest, (iii) evergreen needleaf forest, (iv) C3 grassland, (v) C4 grassland; and (vi) cropland (Table 4). Site data was obtained through the Protocol for the Analysis of Land Surface models (PALS; pals.unsw.edu.au; Abramowitz, 2012) which has previously been pre-processed and quality controlled for use within the LSM community. This process ensured that all site-years had near complete observations of key meteorological drivers (as opposed to significant gap-filled periods). CABLE simulations at the 6 flux sites were not calibrated to match site characteristics; instead default PFT parameters were used, but with the appropriate PFT type for each site.

We next performed global offline simulations using the second Global Soil Wetness Project (GSWP-2) forcing over the period 1986–1995 at a resolution of 1° by 1° with a 30 year spin-up. Although CABLE has the ability to simulate carbon pool dynamics, this feature was not activated for this study, given the relatively short simulation periods. For both the site-scale and global simulations, LAI was prescribed using CABLE's gridded monthly LAI climatology derived from Moderate-resolution Imaging Spectroradiometer (MODIS) LAI data. The GSWP-2 driven simulation used the soil and vegetation parameters similar to those employed when CABLE is coupled to the ACCESS coupled model, rather than those provided by the GSWP-2 experimental protocol. This

was to ensure consistency with future coupled simulations using the new stomatal conductance parameterisation.

2.4 Data sets

2.4.1 LandFlux-EVAL

The LandFlux-EVAL dataset (Mueller et al., 2013) provides a comprehensive ensemble of global evapotranspiration (ET) estimates at a 1° by 1° resolution over the periods 1989–1995 and 1989–2005, derived from various satellites, LSMs driven with observationally based forcing, and atmospheric re-analysis. We used the ensemble combined product (i.e. all sources of ET and associated SD) over the period 1989–1995 as it overlapped with the GSWP-2 forcing period. The rationale for comparing the simulated ET against the LandFlux-EVAL ET was to test that the uncertainties propagated to the ET estimates based on the parameterisation of g_1, were within the uncertainty range of the ensemble of existing models and observational estimates.

2.4.2 GLEAM ET

While zonal mean comparisons provide a useful measure of uncertainty, it is also useful to identify regions where the model deviates more strongly from more observational estimates. We therefore compared the gridded simulated seasonal ET against the latest version of the GLEAM ET product (Miralles et al., 2014). This product is an updated version of the original GLEAM ET (Miralles et al., 2011), that is part of the LandFlux-EVAL ensemble (Mueller et al., 2013). The GLEAM product assimilates multiple satellite observations (temperature, net radiation, precipitation, soil moisture, vegetation water content) into a simple land model to provide estimates of vegetation, soil and total evapotranspiration. Although estimates of vegetation transpiration are available, we only use the total ET product, as the latter has been vigorously evaluated against flux-tower measurements (Miralles et al., 2011, 2014).

2.4.3 Upscaled FLUXNET data

To estimate the influence of the new g_s parameterization on gross primary productivity (GPP), we compared our simulations against the up-scaled FLUXNET model tree ensemble (FLUXNET-MTE) dataset of Jung et al. (2009). This dataset is generated by using outputs from a dynamic global vegetation model (DVGM) forced with gridded observations as the surrogate truth to upscale site-scale quality controlled observations. The product is more reliable where there is a high density of high quality observations, mostly restricted to North America. Nonetheless, the DVGM used to generate this product is one of the most extensively evaluated biosphere models (Jung et al., 2009), and hence is a useful benchmark for our simulations. The FLUXNET dataset provides two version of up-scaled GPP, which differ slightly in how they were derived. We use the mean of the two products.

3 Results

3.1 Single-site results

Figure 3 shows a site-scale comparison during daylight hours (8 a.m.–7 p.m.) between observed and predicted GPP, latent heat flux (LE) and and transpiration (E) at 6 FLUXNET sites. Table 5 shows a series of summary statistics (RMSE, bias and index of agreement) between modelled and observed LE. Differences due to the structure of the model (shown by comparing LEU with MED-L) are small across sites. These small differences indicate that the replacement of the Leuning model with the Medlyn model does not drastically alter CABLE model predictions.

Differences introduced by the PFT parameterisation (MED-P) are most notable at the Howard Springs and Hyytiälä sites. At Hyytiälä, the parameterisation of a conservative water use strategy for needleleaf trees leads to a reduction in both E and LE fluxes (see Table 1) which is consistent with measured FLUXNET data. The differences at

Howard Springs do not stem from the parameterisation, but instead result from assumptions relating to a large positive g_0 parameter in the LEU model (in the default CABLE parameterisation). In these simulations, CABLE (LEU and MED-L) assumes that the site is a C4 grassland and as such, the minimum stomatal conductance g_0 is assumed to equal 0.04 mol m^{-2} leaf s^{-1}. This value is then multiplied by LAI and at the site, can reach values as high as $\sim$ 0.1 mol m^{-2} ground s^{-1}. This value is the minimum over the course of the day. By contrast, in the MED-P model we assumed $g_0 = 0$, meaning that g_s goes to zero under low light and, importantly, high VPD conditions. At Howard Springs high afternoon VPD caused stomatal closure in the MED-P model but not the MED-L or LEU models (Fig. 4). Daily fluxes were thus noticeably lower with the MED-P model. In reality the Howard Springs site is a mixed Eucalypt open forest and C4 grassland (Beringer et al., 2007). The seemingly close agreement between the observed and predicted daily LE fluxes in the LEU model is thus likely a consequence of compensating errors, viz. ignoring the C3 overstorey fluxes and assuming a high g_0, rather than highlighting a problem with the MED-P predictions. In fact, the inferred GPP from the flux site (i.e. net ecosystem exchange + ecosystem respiration) suggests C-uptake fluxes which are at least double those predicted by CABLE (LEU) for the wet season (data not shown).

At Bondville and Cabauw, the MED-P predicts marginally higher peak fluxes as a result of a less conservative water use strategy parameterisation of C3 grasses and crops, respectively. Finally, for the two sites represented by tree PFTs, Harvard and Tumbarumba, the differences between modelled fluxes is negligible. With the exception of Howard Springs, replacing the Leuning model with the MED model and the PFT parameterisation (MED-P) does not have a noticeable impact on predicted fluxes of GPP at any site. GPP is insensitive to the stomatal parameterisation because of the non-linear relationship between g_s and A. When stomata are fully open, A is limited by the rate of ribulose-1,5-bisphosphate (RuBP) regeneration, and is relatively insensitive to the changes in intercellular CO_2 concentration C_i caused by small reductions in stomatal conductance. Finally, it is worth highlighting that the impact of changes in g_s

on fluxes of LE is noticeably smaller than the impact on E and this is because modelled (and observed) LE also includes a flux component from the soil.

3.2 Global results

We next extend this comparison by examining the impact of the MED model on global predictions of GPP and E, the fluxes most directly impacted by g_s in the model. To aid comparisons, Fig. 5 shows the assumed CABLE PFTs across the globe (Lawrence et al., 2012). Figures 6 and 7 show mean seasonal (December-January-February: DJF and June-July-August: JJA) difference maps of predicted GPP and E, respectively. Tables 6 and 7 summarise changes in GPP and E in terms of annual totals across all the GSWP2 years. Similar to Fig. 2, changes in predicted fluxes due to the different models (shown by LEU – MED-L, Figs. 6a, b and 7a, b), are typically small (mean (μ) change relative to the control < 7 %, with the exception of the shrub PFT: $\mu \sim 12$ %). The largest differences occur over grasses (C3 GPP μ = 47.7 g C m^{-2} y^{-1}; C4 GPP μ = 93.0 g C m^{-2} y^{-1}) and shrub PFTs (GPP μ = 69.3 g C m^{-2} y^{-1}), where the LEU model predicts higher fluxes, and across the tropics, where fluxes in broadleaf forest PFTs are higher ($E\mu$ = 34.3 mm y^{-1}) in the MED-L model. In this comparison, model differences result from the different D sensitivities between the models. The difference maps for GPP and E show contrasting spatial patterns. This contrast is related to the strength of the coupling between the vegetation and the surrounding boundary layer. Low stature PFTs (shrubs and grasses) commonly have a low boundary layer conductance. As a result over these PFTs, changes in g_s tend to cause small changes in E fluxes due to boundary layer decoupling, despite there being notable differences in model predictions of GPP.

The key differences introduced by the MED-P model (Figs. 6c, d and 7c, d) are $\sim$ 30 % reduction in E relative to the control simulation for evergreen needleaf (including deciduous needleaf, see caveat below), C4 grass and Tundra PFTs. Fluxes were reduced across the boreal zone ($E\mu$ = 76.1 mm y^{-1}), over C4 grass areas (GPP μ = 302.9 g C m^{-2} y^{-1}; $E\mu$ = 107.7 mm y^{-1}) and the tundra PFT ($E\mu$ = 24.1 mm y^{-1}).

Fluxes are also predicted to decrease over deciduous needleleaf PFTs, but this result should be viewed with caution, as this was the PFT for which there were no synthesis data available. As such, this result just reflects the assumption that these PFTs behave in the same way as evergreen needleleaf PFTs. The MED-P model predicts increases over regions of C3 crop (GPP $\mu = 64.9\,\mathrm{g\,C\,m^{-2}\,y^{-1}}$; $E\mu = 30\,\mathrm{mm\,y^{-1}}$) and C3 grasses (GPP $\mu = 66.8\,\mathrm{g\,C\,m^{-2}\,y^{-1}}$; $E\mu = 17.4\,\mathrm{mm\,y^{-1}}$). Figures 6e, f and 7e, f show the impact of allowing g_1 to vary within a PFT as function of the climate indices. Generally, the changes are in line with the changes introduced by the MED-P parameterisation, with the notable exception of C4 grass pixels. The MED-C model predicts fluxes that are approximately twice those predicted by the MED-P model. This suggests a less conservative water use strategy than is obtained through the stomatal synthesis data alone, i.e. MED-P.

3.3 Comparison with benchmarking products

Global predictions by the CABLE model were then compared to the FLUXNET-MTE and GLEAM ET data products (data not shown). Differences between these data products and CABLE are relatively large and as such, mask the smaller changes in predicted GPP and ET that result from the MED-P/C models. Both products suggest that CABLE over-predicts GPP across the globe and ET across mid-latitudes (20–60° N). The MED-P/C models slightly improve agreement with the FLUXNET-MTE GPP (Table 8) and GLEAM ET for the evergreen needleleaf PFT (Table 9). Agreement is also improved for C4 grasses and Tundra PFTs. However, when considering all PFTs, the MED-P/C models do not noticeably improve agreement with the GLEAM or FLUXNET-MTE products.

Figure 8 shows zonal latitude averages for DJF and JJA compared to the upscaled FLUXNET-MTE GPP and LandFlux-EVAL ET products. As described above, across all latitudes, the differences between the GPP from the data products and those fluxes predicted by the models (LEU, MED-P and MED-C) are generally large and the impact of the new stomatal scheme is typically negligible (Fig. 8a and b). By contrast, the

comparison with ET from the observational data product (Fig. 8c and d) is broadly consistent across all latitudes. Notably, in JJA, the lower ET fluxes predicted by the MED-P/C models across mid (20–60° N) to high latitudes (> 60° N) is in agreement with the LandFlux-EVAL product, though the modelled ET from the MED-L model is not outside the uncertainty envelope of the product. In DJF, the MED-P model also predicts lower GPP and ET fluxes across the tropics (20° S–20° N) which would be towards the low end of the uncertainty envelope from the LandFlux-Eval product, but still falls outside the uncertainty range of the FLUXNET-MTE.

4 Discussion

4.1 Model performance

Stomata are the principal control on the exchange of CO_2 and water vapour in LSMs (Sellers et al., 1996; Dickinson et al., 1998). We tested an implementation of a new stomatal conductance model within the CABLE LSM, at site and global scales to assess the impact on predicted carbon, water and energy fluxes. CABLE is not alone amongst LSMs in only parameterising PFT differences in stomatal behaviour relating to photosynthetic pathway; the Community Land Model version 4.5 (CLM4.5: Oleson et al., 2013) and the ORganizing Carbon and Hydrology in Dynamic EcosystEms model (ORCHIDEE: Krinner et al., 2005), take similar approaches. We utilised a dataset that synthesised stomatal behaviour across the globe in order to constrain the Medlyn model parameter, g_1, by PFT. In addition we tested an empirical model to predict variations in g_1 as a function of growth temperature and aridity.

Introducing the Medlyn g_s model with g_1 parameterisations (MED-P/C) to the CABLE LSM resulted in reductions in E of $\sim 30\,\%$ compared to the standard CABLE simulations across evergreen needleleaf, tundra and C4 grass regions. This large difference represents the conservative behaviour of these PFTs as reported by Lin et al. (2014), currently not captured by the standard CABLE parameters. In other regions of the

globe, the differences between predicted fluxes by the models was typically small. In comparison to alternative estimates from model-data-fusion products, changes in E (or the translation to ET) across mid to high latitudes latitudes, were closer to the mean predictions from the LandFlux-EVAL product, though the MED-L predictions were still within the uncertainty range of the data product. In contrast, across all latitudes the changes introduced by the new stomatal scheme did not improve agreement with the FLUXNET-MTE data product. In comparison with the data products, it was notable that CABLE over-predicted (outside the uncertainty range) GPP across the tropics and predicted ET fluxes lower than the mean, though within the uncertainty envelope. The MED-P model did predict lower GPP fluxes which for this region, which is supported by the data product, but the change was small and still outside of the uncertainty range of the product. Data from Lin et al. (2014) for 3 species in the Amazon suggests that a g_1 value of 4.23 $kPa^{0.5}$ would be appropriate, which is close to the evergreen broadleaf PFT value used in CABLE (4.12 $kPa^{0.5}$). This line of evidence, in combination with the GPP comparison, would tend to suggest that the mismatch between model and data derived ET stems from other biases in the model or forcing data. The issue of bias in predicted fluxes over the Amazon region has previously been identified by Zhang et al. (2013), who argued that the bias was unlikely to result from the forcing data. We cannot resolve this, but this issue warrants further investigation.

An important implication of our results relates to the boreal zone. We cannot explore this fully in uncoupled simulations but this is an important region to the global climate (Bonan et al., 1992) and nutrient cycling (Bonan et al., 1990a, b). Betts (2000) examined how reforestation in this area, while reducing atmospheric CO_2, tended to warm the region due to the masking effect of the forests linked with the snow-albedo feedback. The impacts of the g_1 parameterisation of the Medlyn g_s model on ET over the boreal zone is limited in CABLE because the vegetation is not dynamic and LAI is prescribed. However, our results provide a warning to those modelling this region dynamically using other g_s model parameterisations, which do not explicitly distinguish differences in water use strategy of the vegetation.

4.2 g_1 parameterisation

In this study, we utilised the data collected by Lin et al. (2014) to derive parameter values for g_1 by PFT. In doing so, we have attempted to constrain CABLE's model predictions with the best available gas exchange data. The existing CABLE parameterisation (similar to other LSMs, see above) only considered differences due to photosynthetic pathway and not PFT; furthermore, the origin of this parameterisation has not been well documented in the literature. We also extended the work by Lin et al. (2014), allowing the g_1 parameter to vary within a PFT as a function of growth temperature and aridity. The results shown here are essential a proof of concept, but aptly demonstrate the added "capacity" the Medlyn g_s model may add to CABLE. Unlike the fitted parameters in the current g_s scheme used within CABLE, the g_1 parameter in the Medlyn model has a theoretical interpretation. Héroult et al. (2013) demonstrated a negative correlation between the g_1 parameter and wood density and a positive correlation with the root-to-leaf hydraulic conductance. Lin et al. (2014) examined these relationships with their global stomatal dataset and concluded that such a relationship is consistent across angiosperm tree species but not gymnosperm species. They argued that the discrepancy for the g_1-wood density relationship between angiosperm and gymnosperm tree species results from the evolutional divergence of xylem systems between the two taxa, and thus leads to the difference in their water-use strategies.

Inadequate simulation of soil moisture availability by LSMs is often identified as a key weakness in surface flux prediction (Gedney et al., 2000; Dirmeryer et al., 2006; Lorenz et al., 2012; De Kauwe et al., 2013b). In LSMs, as soil moisture declines, gas exchange is typically reduced through an empirical scalar (Wang et al., 2011) accounting for change in soil water content, but not plant behaviour (isohydric vs. anisohydric) (Egea et al., 2011). Zhou et al. (2013) demonstrated that the g_1 parameter could be linked to a more mechanistic approach to limit gas exchange during water-limited periods, by considering differences in species water use strategies and non-stomatal controls on the apparent maximum rate of carboxylation (V_{cmax}). These studies highlight the

potential to link the g_1 parameter to structural traits within the CABLE model, and/or to hypothesise how g_1 may vary with drought (Zhou et al., 2013), temperature and aridity (shown here by the MED-C simulations).

4.3 Minimum stomatal conductance

For the Medlyn g_s model, we set the minimum stomatal conductance (g_0) to be zero because it is generally small and we did not have data available to estimate it independently of g_1 (Bonan et al., 2014). By contrast, the g_0 parameter within the standard CABLE is assumed to take non-zero leaf-scale values (varying by photosynthetic pathway), which are then scaled to the canopy depending on LAI. These values (g_0 = 0.01 and 0.04 mol m^{-2} s^{-1} for C3 and C4 species respectively) were taken from the Simple Biosphere Model version 2 (SiB2) (Sellers et al., 1996). The original source of these parameter values is unclear. Inspection of data points with low photosynthesis for C4 grasses in the datasets compiled by Lin et al. (2014) suggests that a value in the range 0.01–0.02 mol m^{-2} s^{-1} may be more appropriate. These data are more consistent with parameters used by the CLM4.5 (Oleson et al., 2013) and ORCHIDEE (Krinner et al., 2005) models, which assume g_0 does not vary between photosynthetic pathway (g_0 = 0.02 and g_0 = 0.01 mol m^{-2} s^{-1}, respectively).

As we have shown in the Howard Springs simulations (Figs. 3 and 4), a non-zero g_0 can have a significant impact on ecosystem fluxes. A recent study by Barnard and Bauerle (2013) concluded that g_0 was in fact the most important parameter for correctly estimating transpiration fluxes. It is clear that further work is required on the impact of different g_0 assumptions in land surface and ecosystem models. However, this needs to be done with care. Firstly, values of g_0 should be estimated from data independently of g_1, using stomatal conductance measurements made under low photosynthesis conditions such as low light, high or low temperature, or high VPD. Secondly, values of g_1 then need to be estimated from data with the value of g_0 fixed. It is inappropriate to vary values of g_0 in a model without refitting a corresponding value for g_1. Inspection

of Eq. (4) shows that increasing g_0 without reducing g_1 to compensate will increase stomatal conductance under all conditions, not just low photosynthesis conditions.

4.4 Implications for other models

In this study, we have shown that replacing the empirical Leuning model with the optimisation-based Medlyn model of stomatal conductance has relatively little impact on predicted fluxes. This result is as expected given that the structure of the two models is not dissimilar. Replacing fixed parameter values with values derived from a global stomatal conductance dataset had most impact on prediction of fluxes in boreal and C4 dominated ecosystems. These changes tended overall to improve model performance, although it is clear that there are other sources of bias in the model besides stomatal conductance.

We anticipate that the new stomatal model could also be readily incorporated into other LSMs without degrading performance. However, other models may show more or less sensitivity to the introduction of a new stomatal model, depending on the importance of stomatal resistance in the vegetation–atmosphere pathway. In CABLE, water flow from the vegetation to the atmosphere is controlled by several resistances operating in series, both within the canopy (stomatal and leaf boundary layer conductance) and as turbulent fluxes above the canopy (aerodynamic conductance). CABLE also simulates a sheltering factor to account for the reduced wind speed within the canopy due to leaf sheltering. De Kauwe et al. (2013a) previously identified that CABLE showed stronger levels of decoupling from the boundary layer (Jarvis and McNaughton, 1986) than several other ecosystem and LSMs considered in their model intercomparison. The result of such a decoupling is that changes in E are not proportional to changes in g_s. The small changes in E despite sizeable changes in the g_1 parameterisation observed for several regions in this study suggests a low sensitivity to stomatal parameterisation in these regions, which may arise from high resistances in other parts of the pathway. This is particularly evident for the MED-C simulations in the tropics where the uncertainty in parameterisation was relatively large (Fig. A1) yet

had a small impact on simulated E (Fig. 7). Other models with stronger coupling may show a more important effect in the tropics. However, it is worth noting that a number of studies have suggested forests in the tropics tend to have a high level of decoupling (Meinzer et al., 1997; Wullschleger et al., 1998; Cienciala et al., 2000). It remains unclear whether the multiple layers of resistance to water flow simulated by CABLE are appropriate; this is an area requiring further research.

Other studies may also show larger sensitivity to stomatal parameterisation if they use prognostic LAI. For the simulations carried out here, LAI was prescribed, as is typical in LSMs. In prognostic LAI simulations there may be feedbacks from changes in g_s to LAI that could cause larger differences between the Medlyn and the standard Leuning model, both in terms of the different timings of predicted flux maximums and associated feedbacks on carbon and water fluxes. However, such differences may also be suppressed by the coupling of stomatal conductance with soil moisture. If increases in g_s cause higher ET, soil moisture will be depleted, potentially causing lower ET at a later period. Averaged seasonally, there is therefore a compensatory effect that can minimize the role of g_s in determining ET.

4.5 Optimisation theory in land surface models

In this study we have implemented a simple stomatal conductance formula based on optimisation theory into a LSM. For this test of concept, the parameter values were obtained by fitting the model empirically to data. The model performed as well as, if not better than, previous empirical stomatal models. This result is similar to that of Bonan et al. (2014), who recently implemented a numerical optimal stomatal conductance scheme for the CLM LSM, following Williams et al. (1996). In their implementation they solve numerically the optimisation problem (Eq. 1), with the additional assumption that leaf water potential cannot fall below a minimum value effectively replacing the empirical soil water scalar retained here (Eq. 3). As we did, Bonan et al. (2014) found that model performance using the optimisation scheme was not degraded when compared to the original empirical stomatal conductance scheme (the Ball et al., 1987,

model). However, the analytical solution implemented here has a number of advantages over a numerical optimisation solution, including the smaller computational cost and reduced model complexity. The analytical solution also correctly captures stomatal responses to rising atmospheric CO_2 concentration, whereas the full numerical solution does not – it behaves incorrectly when photosynthesis is limited by Rubisco activity (Medlyn et al., 2011, 2013).

In addition, we have here been able to use the optimisation theory as a basis for model parameterisation. Our implementation of the optimal model has one key parameter, g_1, related to the marginal carbon cost of water; this parameter can be readily and accurately estimated from data. Lin et al. (2014) used theoretical considerations to predict how this parameter should vary among PFTs and with mean annual climate, and used a global g_s database to test these predictions. The resulting parameter values were employed in the LSM and resulted in large changes to predicted fluxes in evergreen needleleaf and C4 vegetation. This work paves the way for broader implementations of optimisation theory in LSMs and other large-scale vegetation models.

Acknowledgements. This work was supported by the Australian Research Council Centre of Excellence for Climate System Science through grant CE110001028, and by ARC Discovery Grant DP DP120104055. This study uses the LandFlux-EVAL merged benchmark synthesis products of ETH Zurich produced under the aegis of the GEWEX and ILEAPS projects (http://www.iac.ethz.ch/groups/seneviratne/research/LandFlux-EVAL). We thank CSIRO and the Bureau of Meteorology through the Centre for Australian Weather and Climate Research for their support in the use of the CABLE model. We thank the National Computational Infrastructure at the Australian National University, an initiative of the Australian Government, for access to supercomputer resources. The up-scaled Fluxnet dataset was provided by Martin Jung from the Max Planck Institute for Biogeochemistry. This work used eddy covariance data acquired by the FLUXNET community for the La Thuile FLUXNET release, supported by the following networks: AmeriFlux (US Department of Energy, Biological and Environmental Research, Terrestrial Carbon Program (DE-FG02-04ER63917 and DE-FG02-04ER63911)), AfriFlux, AsiaFlux, CarboAfrica, CarboEuropeIP, CarboItaly, CarboMont, ChinaFlux, Fluxnet-Canada (supported by CFCAS, NSERC, BIOCAP, Environment Canada, and NRCan), GreenGrass, KoFlux, LBA, NECC, OzFlux, TCOS-Siberia, USCCC. We acknowledge the financial support to the

eddy covariance data harmonization provided by CarboEuropeIP, FAO-GTOS-TCO, iLEAPS, Max Planck Institute for Biogeochemistry, National Science Foundation, University of Tuscia, Université Laval and Environment Canada and US Department of Energy and the database development and technical support from Berkeley Water Center, Lawrence Berkeley National Laboratory, Microsoft Research eScience, Oak Ridge National Laboratory, University of California – Berkeley, University of Virginia. All data analysis and plots were generated using the Python language and the Matplotlib Basemap Toolkit (Hunter, 2007).

References

Abramowitz, G.: Towards a public, standardized, diagnostic benchmarking system for land surface models, Geosci. Model Dev., 5, 819–827, doi:10.5194/gmd-5-819-2012, 2012.

Abramowitz, G., Leuning, R., Clark, M., and Pitman, A.: Evaluating the performance of land surface models, J. Climate, 21, 5468–5481, 2008.

Aphalo, P. and Jarvis, P.: Do stomata respond to relative humidity?, Plant Cell Environ., 14, 127–132, 1991.

Arneth, A., Lloyd, J., Šantrůčková, H., Bird, M., Grigoryev, S., Kalaschnikov, Y., Gleixner, G., and Schulze, E.-D.: Response of central Siberian Scots pine to soil water deficit and long-term trends in atmospheric CO_2 concentration, Global Biogeochem. Cy., 16, 5–1, 2002.

Ball, M. C., Woodrow, I. E., and Berry, J. A.: Progress in Photosynthesis Research, edited by: Biggins, I., Martinus Nijhoff Publisheres, Netherlands, 221–224, 1987.

Barnard, D. and Bauerle, W.: The implications of minimum stomatal conductance on modeling water flux in forest canopies, J. Geophys. Res.-Biogeo., 118, 1322–1333, 2013.

Beringer, J., Hutley, L. B., Tapper, N. J., and Cernusak, L. A.: Savanna fires and their impact on net ecosystem productivity in North Australia, Glob. Change Biol., 13, 990–1004, 2007.

Betts, R. A.: Offset of the potential carbon sink from boreal forestation by decreases in surface albedo, Nature, 408, 187–190, 2000.

Betts, R. A., Boucher, O., Collins, M., Cox, P. M., Falloon, P. D., Gedney, N., Hemming, D. L., Huntingford, C., Jones, C. D., Sexton, D. M., and Webb, M. J.: Projected increase in continental runoff due to plant responses to increasing carbon dioxide, Nature, 448, 1037–1041, 2007.

Bonan, G. B.: Carbon and nitrogen cycling in North American boreal forests, Biogeochemistry, 10, 1–28, 1990a.

Bonan, G. B.: Carbon and nitrogen cycling in North American boreal forests. II. Biogeographic patterns, Can. J. Forest Res., 20, 1077–1088, 1990b.

Bonan, G. B., Pollard, D., and Thompson, S. L.: Effects of boreal forest vegetation on global climate, Nature, 359, 716–718, 1992.

Bonan, G. B., Williams, M., Fisher, R. A., and Oleson, K. W.: Modeling stomatal conductance in the earth system: linking leaf water-use efficiency and water transport along the soil–plant–atmosphere continuum, Geosci. Model Dev., 7, 2193–2222, doi:10.5194/gmd-7-2193-2014, 2014.

Buckley, T., Mott, K., and Farquhar, G.: A hydromechanical and biochemical model of stomatal conductance, Plant Cell Environ., 26, 1767–1785, 2003.

Cao, L., Bala, G., Caldeira, K., Nemani, R., and Ban-Weiss, G.: Importance of carbon dioxide physiological forcing to future climate change, P. Natl. Acad. Sci. USA, 107, 9513–9518, 2010.

Cienciala, E., Kučera, J., and Malmer, A.: Tree sap flow and stand transpiration of two *Acacia mangium* plantations in Sabah, Borneo, J. Hydrol., 236, 109–120, 2000.

Cowan, I.: On the Economy of Plant Form and Function, edited by: Givnish, T. J., Cambridge University Press, 133–171, 1986.

Cowan, I. and Farquhar, G.: Stomatal Function in Relation to Leaf Metabolism and Environment, Symposia of the Society for Experimental Biology, 471 pp., 1977.

Cruz, F. T., Pitman, A. J., and Wang, Y.-P.: Can the stomatal response to higher atmospheric carbon dioxide explain the unusual temperatures during the 2002 Murray–Darling Basin drought?, J. Geophys. Res.-Atmos., 115, D02101, doi:10.1029/2009JD012767, 2010.

Damour, G., Simonneau, T., Cochard, H., and Urban, L.: An overview of models of stomatal conductance at the leaf level, Plant Cell Environ., 33, 1419–1438, 2010.

De Kauwe, M. G., Medlyn, B. E., Zaehle, S., Walker, A. P., Dietze, M. C., Hickler, T., Jain, A. K., Luo, Y., Parton, W. J., Prentice, I. C., Smith, B., Thornton, P. E., Wang, S., Wang, Y.-P., Warlind, D., Weng, E., Crous, K. Y., Ellsworth, D. S., Hanson, P. J., Seok Kim, H., Warren, J. M., Oren, R., and Norby, R. J.: Forest water use and water use efficiency at elevated CO_2: a model-data intercomparison at two contrasting temperate forest FACE sites, Glob. Change Biol., 19, 1759–1779, 2013a.

De Kauwe, M. G., Taylor, C. M., Harris, P. P., Weedon, G. P., and Ellis, R. J.: Quantifying land surface temperature variability for two Sahelian mesoscale regions during the wet season, J. Hydrometeorol., 14, 1605–1619, 2013b.
Dickinson, R. E., Shaikh, M., Bryant, R., and Graumlich, L.: Interactive canopies for a climate model, J. Climate, 11, 2823–2836, 1998.
Egea, G., Verhoef, A., and Vidale, P. L.: Towards an improved and more flexible representation of water stress in coupled photosynthesis–stomatal conductance models, Agr. Forest Meteorol., 151, 1370–1384, 2011.
Farquhar, G. D. and Sharkey, T. D.: Stomatal conductance and photosynthesis, Annu. Rev. Plant Physio., 33, 317–345, 1982.
Gallego-Sala, A., Clark, J., House, J., Orr, H., Prentice, I. C., Smith, P., Farewell, T., and Chapman, S.: Bioclimatic envelope model of climate change impacts on blanket peatland distribution in Great Britain, Clim. Res., 45, 151–162, 2010.
Gedney, N., Cox, P., Douville, H., Polcher, J., and Valdes, P.: Characterizing GCM land surface schemes to understand their responses to climate change, J. Climate, 13, 3066–3079, 2000.
Gedney, N., Cox, P., Betts, R., Boucher, O., Huntingford, C., and Stott, P.: Detection of a direct carbon dioxide effect in continental river runoff records, Nature, 439, 835–838, 2006.
Hari, P., Mäkelä, A., Korpilahti, E., and Holmberg, M.: Optimal control of gas exchange, Tree Physiol., 2, 169–175, 1986.
Henderson-Sellers, A., McGuffie, K., and Gross, C.: Sensitivity of global climate model simulations to increased stomatal resistance and CO_2 increases, J. Climate, 8, 1738–1756, 1995.
Héroult, A., Lin, Y.-S., Bourne, A., Medlyn, B. E., and Ellsworth, D. S.: Optimal stomatal conductance in relation to photosynthesis in climatically contrasting Eucalyptus species under drought, Plant Cell Amp Environ., 36, 262–274, 2013.
Hunter, J. D.: Matplotlib: a 2D graphics environment, Comput. Sci. Amp Eng., 9, 90–95, 2007.
Jarvis, P. and McNaughton, K.: Stomatal control of transpiration: scaling up from leaf to region, Adv. Ecol. Res., 15, 1–49, 1986.
Jung, M., Reichstein, M., and Bondeau, A.: Towards global empirical upscaling of FLUXNET eddy covariance observations: validation of a model tree ensemble approach using a biosphere model, Biogeosciences, 6, 2001–2013, doi:10.5194/bg-6-2001-2009, 2009.
Kala, J., Decker, M., Exbrayat, J.-F., Pitman, A. J., Carouge, C., Evans, J. P., Abramowitz, G., and Mocko, D.: Influence of leaf area index prescriptions on simulations of heat, moisture, and carbon fluxes, J. Hydrometeorol., 15, 489–503, 2014.

Katul, G. G., Palmroth, S., and Oren, R.: Leaf stomatal responses to vapour pressure deficit under current and CO_2-enriched atmosphere explained by the economics of gas exchange, Plant Cell Environ., 32, 968–979, 2009.
Kerstiens, G.: Cuticular water permeability and its physiological significance, J. Exp. Bot., 47, 1813–1832, 1996.
Kowalczyk, E. A., Wang, Y. P., Wang, P., Law, R. H., and Davies, H. L.: The CSIRO Atmosphere Biosphere Land Exchange (CABLE) model for use in climate models and as an offline model (No. CSIRO Marine and Atmospheric Research 013), CSIRO, 2006.
Kowalczyk, E. A., Stevens, L., Law, R. M., Dix, M. D., Wang, Y.-P., Harman, I. N., Haynes, K., Srbinovsky, J., Pak, B., and Ziehn, T.: The land surface model component of ACCESS: description and impact on the simulated surface climatology, Australian Meteorological and Oceanographic Journal, 63, 65–82, 2013.
Krinner, G., Viovy, N., de Noblet-Ducoudré, N., Ogée, J., Polcher, J., Friedlingstein, P., Ciais, P., Sitch, S., and Prentice, I. C.: A dynamic global vegetation model for studies of the coupled atmosphere–biosphere system, Global Biogeochem. Cy., 19, GB1015, doi:10.1029/2003GB002199, 2005.
Leuning, R.: A critical appraisal of a combined stomatal-photosynthesis model for C3 plants, Plant Cell Environ., 18, 339–355, 1995.
Lin, Y.-S., Medlyn, B. E., Duursma, R. A., Prentice, I. C., Wang, H., Baig, S., Eamus, D., Resco de Dios, V. Mitchell, P., Ellsworth, D. S., Op de Beeck, M., Wallin, G., Uddling, J., Tarvainen, L., Linderson, M.-J., Cernusak, L. A., Nippert, J. B., Ocheltree, T. W., Tissue. D. T., Martin-StPaul, N. K., Rogers, A., Warren, J. M., De Angelis, P, Hikosaka, K., Han, Q., Onoda, Y., Gimeno, T. E., Barton, C. V. M., Bennie, J., Bonal, D., Bosc, A., Löw, M., Macinins-Ng, C., Rey, A., Rowland, L., Setterfield, S. A., Tausz-Posch, S., Zaragoza-Castells, J., Broadmeadow, M. S. J., Drake, J. E., Freeman, M., Ghannoum, O., Hutley, L. B., Kelly, J. W., Kikuzawa, K., Kolari, P., Koyama, K., Limousin, J- M., Meir, P., Lola da Costa, A. C., Mikkelsen, T. N., Salinas, N., and Sun, W.: Optimal stomatal behaviour around the world: synthesis of a global stomatal conductance database, in review, 2014.
Lloyd, J.: The CO_2 dependence of photosynthesis, plant growth responses to elevated CO_2 concentrations and their interaction with soil nutrient status, II. Temperate and boreal forest productivity and the combined effects of increasing CO_2 concentrations and increased nitrogen deposition at a global scale, Funct. Ecol., 13, 439–459, 1999.

Lorenz, R., Pitman, A. J., Donat, M. G., Hirsch, A. L., Kala, J., Kowalczyk, E. A., Law, R. M., and Srbinovsky, J.: Representation of climate extreme indices in the ACCESS1.3b coupled atmosphere–land surface model, Geosci. Model Dev., 7, 545–567, doi:10.5194/gmd-7-545-2014, 2014.

Medlyn, B. E., Duursma, R. A., Eamus, D., Ellsworth, D. S., Prentice, I. C., Barton, C. V. M., Crous, K. Y., De Angelis, P., Freeman, M., and Wingate, L.: Reconciling the optimal and empirical approaches to modelling stomatal conductance, Glob. Change Biol., 17, 2134–2144, 2011.

Medlyn, B. E., Duursma, R. A., De Kauwe, M. G., and Prentice, I. C.: The optimal stomatal response to atmospheric CO_2 concentration: alternative solutions, alternative interpretations, Agr. Forest Meteorol., 182–183, 200–203, 2013.

Meinzer, F., Andrade, J., Goldstein, G., Holbrook, N., Cavelier, J., and Jackson, P.: Control of transpiration from the upper canopy of a tropical forest: the role of stomatal, boundary layer and hydraulic architecture components, Plant Cell Environ., 20, 1242–1252, 1997.

Miralles, D. G., De Jeu, R. A. M., Gash, J. H., Holmes, T. R. H., and Dolman, A. J.: Magnitude and variability of land evaporation and its components at the global scale, Hydrol. Earth Syst. Sci., 15, 967–981, doi:10.5194/hess-15-967-2011, 2011.

Miralles, D., van den Berg, M., Gash, J., Parinussa, R., de Jeu, R., Beck, H., Holmes, D., Jimenez, C., Verhoest, N., Dorigo, W., Teuling, A. J., and Dolman, J.: El Niño–La Niña cycle and recent trends in continental evaporation, Nature Clim. Change, 4, 122–126, 2014.

Mott, K. and Parkhurst, D.: Stomatal responses to humidity in air and helox, Plant Cell Environ., 14, 509–515, 1991.

Mueller, B., Hirschi, M., Jimenez, C., Ciais, P., Dirmeyer, P. A., Dolman, A. J., Fisher, J. B., Jung, M., Ludwig, F., Maignan, F., Miralles, D. G., McCabe, M. F., Reichstein, M., Sheffield, J., Wang, K., Wood, E. F., Zhang, Y., and Seneviratne, S. I.: Benchmark products for land evapotranspiration: LandFlux-EVAL multi-data set synthesis, Hydrol. Earth Syst. Sci., 17, 3707–3720, doi:10.5194/hess-17-3707-2013, 2013.

Oleson, K. W., Lawrence, D. M., Bonan, G. B., Drewniak, B., Huang, M., Koven, C. D., Levis, S., Li, F., Riley, W. J., Subin, Z. M., Swenson, S. C., Thornton, P. E., Bozbiyik, A., Fisher, R., Heald, C. L., Kluzek, E., Lamarque, J.-F., Lawrence, P. J., Leung, L. R., Lipscomb, W., Muszala, S., Ricciuto, D. M., Sacks, W., Sun, Y., Tang, J., and Yang, Z.-L.: Technical Description of version 4.5 of the Community Land Model (CLM) (NCAR Technical Note No.

NCAR/TN-503+STR), Citeseer, National Center for Atmospheric Research, Boulder, Colorado, 2013.

Pitman, A.: The evolution of, and revolution in, land surface schemes designed for climate models, Int. J. Climate, 23, 479–510, 2003.

Pollard, D. and Thompson, S. L.: Use of a land-surface-transfer scheme (LSX) in a global climate model: the response to doubling stomatal resistance, Glob. Planet. Change, 10, 129–161, 1995.

Raupach, M.: Simplified expressions for vegetation roughness length and zero-plane displacement as functions of canopy height and area index, Bound.-Lay. Meteorol., 71, 211–216, 1994.

Raupach, M., Finkele, K., and Zhang, L.: SCAM (Soil–Canopy–Atmosphere Model): Description and Comparison with Field Data, Aust. Csiro Cem Tech. Rep. 81, Aspendale, 1997.

Schymanski, S. J., Sivapalan, M., Roderick, M. L., Hutley, L. B., and Beringer, J.: An optimality-based model of the dynamic feedbacks between natural vegetation and the water balance, Water Resour. Res., 45, W01412, doi:10.1029/2008WR006841, 2009.

Sellers, P., Bounoua, L., Collatz, G., Randall, D., Dazlich, D., Los, S., Berry, J., Fung, I., Tucker, C., Field, C., and Jensen, T. G.: Comparison of radiative and physiological effects of doubled atmospheric CO_2 on climate, Science, 271, 1402–1406, 1996.

R Core Development Team: R: a Language and Environment for Statistical Computing, R Foundation for Statistical Computing, Vienna, Austria, 2013.

Wang, Y. P. and Leuning, R.: A two-leaf model for canopy conductance, photosynthesis and partitioning of available energy I: Model description and comparison with a multi-layered model, Agr. Forest Meteorol., 91, 89–111, 1998.

Wang, Y. P., Kowalczyk, E., Leuning, R., Abramowitz, G., Raupach, M. R., Pak, B., van Gorsel, E., and Luhar, A.: Diagnosing errors in a land surface model (CABLE) in the time and frequency domains, J. Geophys. Res.-Biogeo., 116, G01034, doi:10.1029/2010JG001385, 2011.

Wang, Y., Papanatsiou, M., Eisenach, C., Karnik, R., Williams, M., Hills, A., Lew, V. L., and Blatt, M. R.: Systems dynamic modeling of a guard cell Cl – channel mutant uncovers an emergent homeostatic network regulating stomatal transpiration, Plant Physiol., 160, 1956–1967, 2012.

Wullschleger, S. D., Meinzer, F., and Vertessy, R.: A review of whole-plant water use studies in tree, Tree Physiol., 18, 499–512, 1998.

Zhang, Q., Pitman, A. J., Wang, Y. P., Dai, Y. J., and Lawrence, P. J.: The impact of nitrogen and phosphorous limitation on the estimated terrestrial carbon balance and warming of land use change over the last 156 yr, Earth Syst. Dynam., 4, 333–345, doi:10.5194/esd-4-333-2013, 2013.

Zhou, S., Duursma, R. A., Medlyn, B. E., Kelly, J. W., and Prentice, I. C.: How should we model plant responses to drought? An analysis of stomatal and non-stomatal responses to water stress, Agr. Forest Meteorol., 182–183, 204–214, 2013.

Table 1. Fitted g_1 values based on the CABLE PFTs using data from Lin et al. (2014).

PFT	g_1 mean ($kPa^{0.5}$)	g_1 standard error ($kPa^{0.5}$)
Evergreen needleleaf	2.35	0.25
Evergreen broadleaf	4.12	0.09
Deciduous needleleaf	2.35	0.25
Deciduous broadleaf	4.45	0.36
Shrub	4.70	0.82
C3 grassland	5.25	0.32
C4 grassland	1.62	0.13
Tundra	2.22	0.4
C3 cropland	5.79	0.64

Table 2. Model coefficients used in mixed effects model to predict g_1 from two long-term average (1960–1990) bioclimatic variables: temperature and a moisture index representing an indirect estimate of plant water availability.

PFT	*a*	*b*	*c*	*d*	*e*
Evergreen needleleaf	1.32	0.03	0.02	0.01	−0.97
Evergreen broadleaf	1.32	0.03	0.02	0.01	−0.67
Deciduous needleleaf	1.32	0.03	0.02	0.01	−0.97
Deciduous broadleaf	1.32	0.03	0.02	0.01	−0.37
Shrub	1.32	0.03	0.02	0.01	−0.29
C3 grassland	1.32	0.03	0.02	0.01	−0.1
C4 grassland	1.32	0.03	0.02	0.01	−1.35
Tundra	1.32	0.03	0.02	0.01	−0.73
C3 cropland	1.32	0.03	0.02	0.01	0.0

Table 3. A summary of model simulations.

Model Simulation	Description
LEU	Control experiment, standard CABLE model with the Leuning g_s model.
MED-L	Medlyn model with parameters (g_0 and g_1) calibrated against an offline Leuning model.
MED-P	Medlyn model with the g_1 parameter calibrated by PFT constrained by a global synthesis of stomatal data.
MED-C	Medlyn model with the g_1 parameters predicted from a mixed effects model considering the impacts of temperature and aridity.

Table 4. Summary of flux tower sites.

Site	FLUXNET Vegetation Type	CABLE PFT	Latitude	Longitude	Country	Years
Bondville	Cropland	C3 Crop	40.00° N	−88.29° W	US	1997–2006
Cabauw	Grassland	C3 Grass	51.97° N	4.93° E	Holland	2003–2006
Harvard	Deciduous broadleaf	Deciduous broadleaf	42.54° N	−72.17° W	US	1994–2001
Howard Springs	Woody Savannah	C4 grass	−12.49° S	131.15° E	Australia	2002–2005
Hyytiala	Evergreen needleleaf	Evergreen needleleaf	61.85° N	23.29° E	Finland	2001–2004
Tumbarumba	Evergreen broadleaf	Evergreen broadleaf	−35.66° S	148.15° E	Australia	2002–2005

Table 5. Summary statistics of modelled and observed LE at the 6 FLUXNET sites during daylight hours (9 a.m.–18 p.m.) and over the peak-growing season (for Northern Hemisphere sites, from June-July-August and for Southern Hemisphere sites, from December-January-February).

Site	RMSE			Bias			Index of Agreement		
	LEU	MED-L	MED-P	LEU	MED-L	MED-P	LEU	MED-L	MED-P
Bondville	109.91	102.74	109.78	−12.92	−9.50	−5.80	0.81	0.83	0.84
Cabauw	82.13	78.65	82.76	−13.54	−13.15	−12.75	0.78	0.80	0.79
Harvard	59.17	55.51	58.51	8.35	4.10	7.10	0.94	0.95	0.95
Howard Springs	105.92	105.72	138.57	−4.86	1.16	−61.25	0.83	0.84	0.62
Hyytiala	58.90	54.62	47.33	21.00	16.26	−0.24	0.89	0.89	0.89
Tumbarumba	130.91	124.28	124.84	−15.06	−14.30	−13.22	0.76	0.78	0.78

Table 6. Mean difference in GPP between the LEU and MED-L model, the LEU and MED-P models and the LEU-C models for each of CABLE's PFTs.

PFT	GPP: LEU – MED-L ($g C m^{-2} y^{-1}$)	GPP: LEU – MED-P ($g C m^{-2} y^{-1}$)	GPP: LEU – MED-C ($g C m^{-2} y^{-1}$)
Evergreen needleleaf	−3.08 ± 18.39	39.05 ± 34.18	43.45 ± 24.2
Evergreen broadleaf	36.1 ± 51.93	76.12 ± 61.99	73.70 ± 65.08
Deciduous needleleaf	−1.84 ± 5.14	24.06 ± 5.35	34.03 ± 5.75
Deciduous broadleaf	−31.48 ± 57.77	−17.31 ± 38.	−46.3 ± 69.01
Shrub	−69.28 ± 32.31	−45.46 ± 17.61	−35.39 ± 17.41
C3 grassland	−47.73 ± 46.83	−66.76 ± 41.55	−62.79 ± 50.02
C4 grassland	−93.04 ± 45.95	302.94 ± 113.93	115.53 ± 89.29
Tundra	0.3 ± 12.63	16.61 ± 14.16	13.36 ± 11.02
C3 cropland	−26.85 ± 36.51	−64.93 ± 36.58	−65.45 ± 58.21

Table 7. Mean difference in E between the LEU and MED-L model, the LEU and MED-P models and the LEU-C models for each of CABLE's PFTs.

PFT	E: LEU – MED-L ($mm y^{-1}$)	E: LEU – MED-P ($mm y^{-1}$)	E: LEU – MED-C ($mm y^{-1}$)
Evergreen needleleaf	16.55 ± 9.78	76.27 ± 36.34	81.72 ± 29.36
Evergreen broadleaf	34.34 ± 14.34	27.31 ± 14.7	22.66 ± 48.16
Deciduous needleleaf	10.5 ± 6.18	54.36 ± 17.07	67.03 ± 17.83
Deciduous broadleaf	11.15 ± 13.61	0.56 ± 8.45	−10.16 ± 34.36
Shrub	−11.14 ± 5.2	−4.81 ± 5.51	−1.68 ± 6.21
C3 grassland	0.34 ± 10.68	−17.37 ± 8.63	−15.51 ± 19.63
C4 grassland	−11.99 ± 5.67	107.77 ± 41.88	47.34 ± 32.21
Tundra	5.9 ± 3.87	24.13 ± 14.38	20.96 ± 11.75
C3 cropland	0.8 ± 12.37	−30.07 ± 12.36	−28.56 ± 30.11

Table 8. Summary statistics for December-January-February (DJF) June-July-August (JJA), describing the root mean squared error (RMSE) and bias between the FLUXNET-MTE GPP product and the CABLE model.

PFT	LEU (JJA; DJF)		MED-P (JJA; DJF)		MED-C (JJA; DJF)	
	RMSE	Bias	RMSE	Bias	RMSE	Bias
Evergreen needleleaf	3.23; 0.4	2.73; 0.11	2.98; 0.39	2.42; 0.1	2.92; 0.39	2.37; 0.1
Evergreen broadleaf	2.31; 2.29	1.87; 1.57	2.14; 2.16	1.66; 1.36	2.12; 2.09	1.68; 1.36
Deciduous needleleaf	4.41; 0.00	4.37; 0.00	4.17; 0.00	4.13; 0.00	4.07; 0.00	4.03; 0.00
Deciduous broadleaf	2.33; 1.81	1.75; 1.27	2.33; 1.88	1.78; 1.33	2.35; 1.97	1.82; 1.42
Shrub	0.98; 0.86	0.72; 0.51	1.10; 0.95	0.84; 0.61	1.08; 0.91	0.82; 0.57
C3 grassland	1.86; 1.44	1.37; 0.85	2.09; 1.57	1.67; 0.97	2.06; 1.59	1.61; 0.99
C4 grassland	3.15; 2.36	2.55; 1.73	2.43; 1.67	1.77; 0.94	2.94; 2.16	2.24; 1.43
Tundra	2.48; 0.29	1.79; 0.03	2.31; 0.27	1.62; 0.03	2.34; 0.27	1.66; 0.03
C3 cropland	1.96; 1.25	1.33; 0.83	2.18; 1.39	1.64; 0.94	2.13; 1.43	1.59; 0.96

Table 9. Summary statistics for December-January-February (DJF) June-July-August (JJA), describing the root mean squared error (RMSE) and bias between the GLEAM ET product and the CABLE model.

PFT	LEU (JJA; DJF)		MED-P (JJA; DJF)		MED-C (JJA; DJF)	
	RMSE	Bias	RMSE	Bias	RMSE	Bias
Evergreen needleleaf	2.37; 1.83	0.79; 0.24	2.28; 1.83	0.31; 0.23	2.27; 1.83	0.26; 0.23
Evergreen broadleaf	2.17; 2.32	−0.05; −0.25	2.18; 2.34	−0.12; −0.32	2.17; 2.32	−0.1; −0.31
Deciduous needleleaf	1.45; 0.69	1.15; −0.02	1.19; 0.69	0.75; −0.02	1.13; 0.69	0.65; −0.0
Deciduous broadleaf	2.69; 2.43	0.79; 0.58	2.69; 2.43	0.77; 0.58	2.69; 2.43	0.78; 0.61
Shrub	1.25; 1.34	0.29; 0.47	1.24; 1.34	0.29; 0.46	1.25; 1.34	0.29; 0.45
C3 grassland	1.66; 1.49	0.53; 0.34	1.67; 1.5	0.55; 0.36	1.67; 1.5	0.54; 0.37
C4 grassland	1.37; 1.38	0.33; 0.29	1.32; 1.35	0.2; 0.09	1.35; 1.35	0.29; 0.2
Tundra	2.35; 1.88	0.74; 0.37	2.31; 1.88	0.55; 0.36	2.31; 1.88	0.57; 0.36
C3 cropland	1.8; 1.38	0.9; 0.29	1.85; 1.39	0.98; 0.3	1.84; 1.39	0.97; 0.3

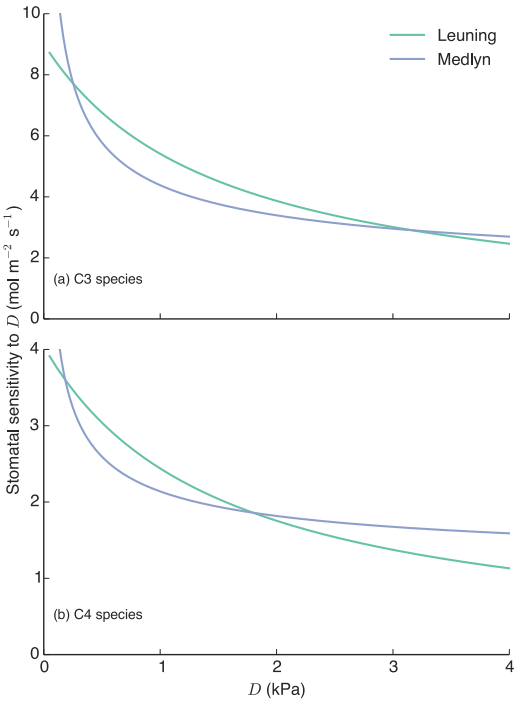

Figure 1. Stomatal sensitivity to increased vapour pressure deficit (D). The Leuning model has been parameterised in the same way as the CABLE model, for C3 species: g_0 = 0.01 mol m^{-2} s^{-1}, a_1 = 9.0, D = 1.5 kPa and for C4 plants: g_0 = 0.04 mol m^{-2} s^{-1}, a_1 = 4.0, D_0 = 1.5 kPa. The Medlyn model has been fit to output generated by the Leuning model using least squares for D ranging from 0.05 to 3 kPa. The calibrated parameters for the Medlyn model were g_1 = 3.88 and g_1 = 1.22 for C3 and C4 species, respectively.

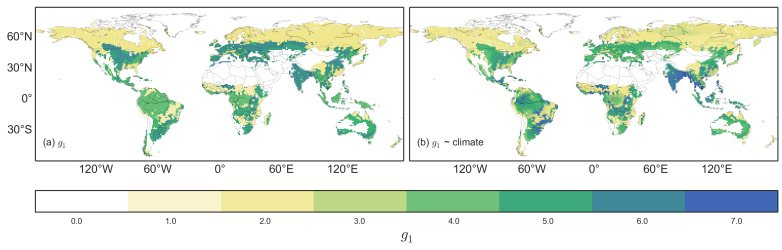

Figure 2. Global maps showing how the g_1 model parameter varies across the globe. **(a)** shows the fitted g_1 parameter values for each PFT based on the data, whilst **(b)** shows the predicted g_1 parameter values considering the influence of climate indices. In total, 126 pixels have been masked from **(b)**, representing pixels where the temperature range and moisture index extended outside the range of the synthesis g_s database.

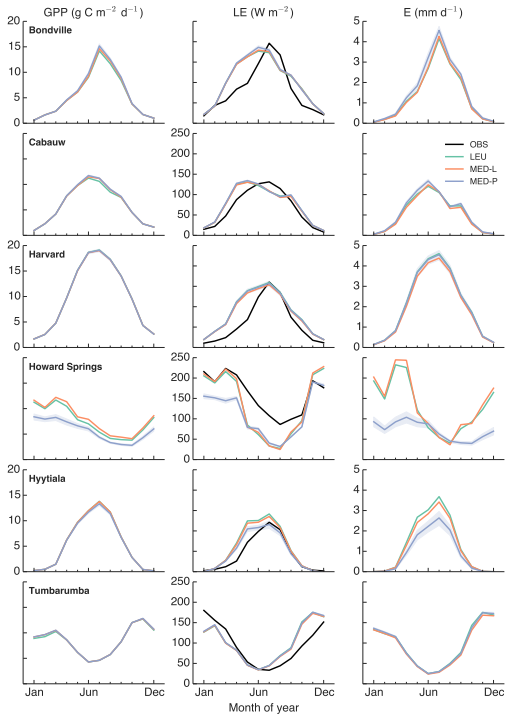

Figure 3. A comparison of the observed (OBS) and modelled average seasonal cycle of gross primary productivity (GPP), Latent Heat (LE) and transpiration (E) at 6 FLUXNET sites during daylight hours (8 a.m.–7 p.m.). Timeseries have been averaged across all years as described in Table 4 to produce seasonal cycles. Light blue shading indicates the uncertainty in predicted fluxes from the Medlyn model (MED-P), accounting for ±2 standard errors in the site g_1 parameter value.

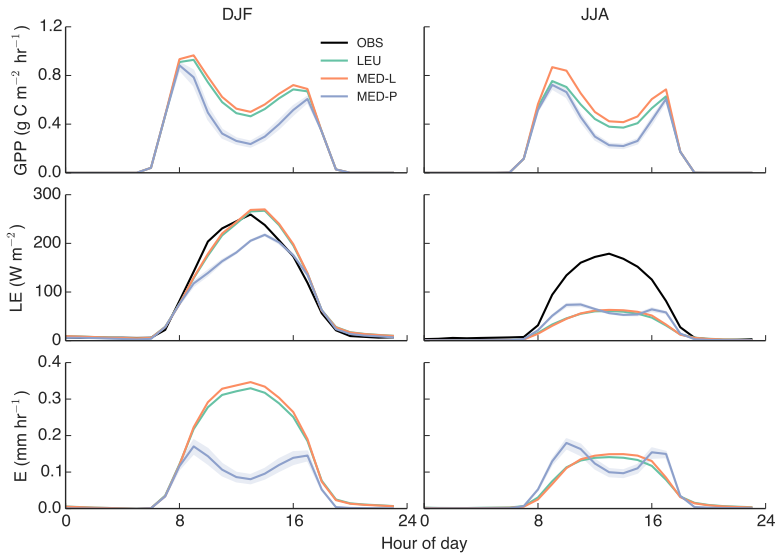

Figure 4. Mean diurnal observed (OBS) and modelled gross primary productivity (GPP), Latent Heat (LE) and transpiration (E) at the Howard Springs Fluxnet sites during daylight hours (8 a.m.–7 p.m.). Timeseries have been averaged across all years as described in Table 2 to produce diurnal seasonal cycles. Light blue shading indicates the uncertainty in predicted fluxes from the Medlyn model (MED-P), accounting for ±2 standard errors in the site g_1 parameter value.

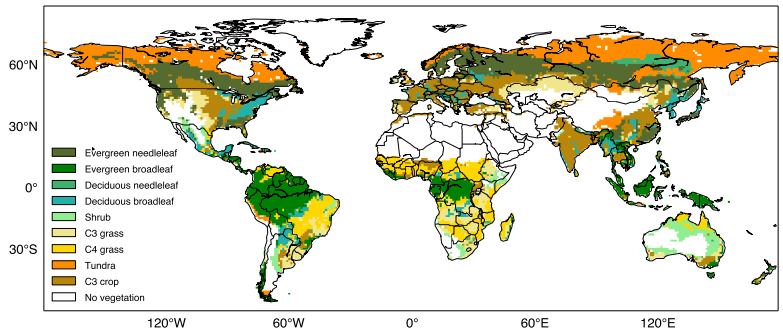

Figure 5. Map showing the plant functional types (PFTs) currently used in the CABLE model. CABLE also has C4 crop, wetland and urban PFTs, however these are currently not operational.

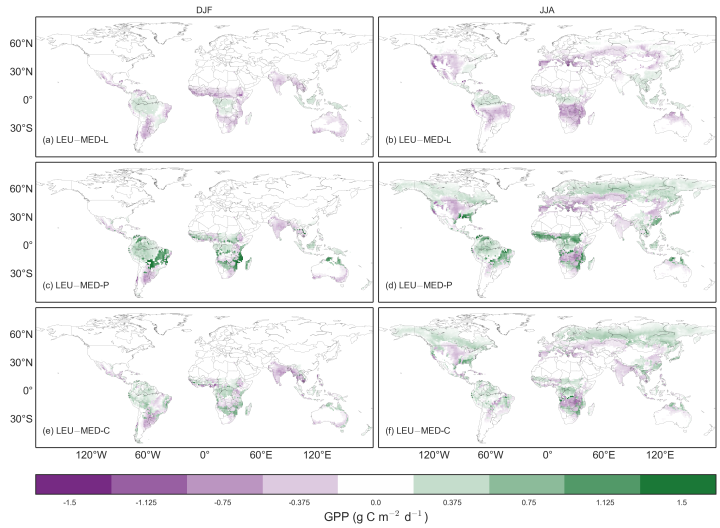

Figure 6. Mean seasonal (December-January-February: DJF and June-July-August: JJA) difference maps of gross primary productivity (GPP) calculated across the 10 years of the Global Soil Wetness Project2 (GSWP2) forcing (1986–1995) period. **(a)** and **(b)** show the difference between the standard CABLE (LEU) model and the Medlyn model fit to the Leuning model (MED-L), **(c)** and **(d)** show the difference between the LEU model and the Medlyn model with the g_1 PFT parameterisation (MED-P), and finally, **(e)** and **(f)** show the difference between the LEU model and the Medlyn model with the g_1 parameter predicted as a function of climate indices (MED-C). In total, 126 pixels have been masked from **(e)** and **(f)**, representing pixels where the temperature range and moisture index extended outside the range of the synthesis g_s database. Data shown in **(b–f)** have been clipped, with the maximum ranges extending to (−1.6–0.36), (−1.28–3.03), (−1.19–3.82), (−1.2–2.9) and (−1.05–3.7) and this affects 1, 64, 34, 42 and 147 pixels, respectively.

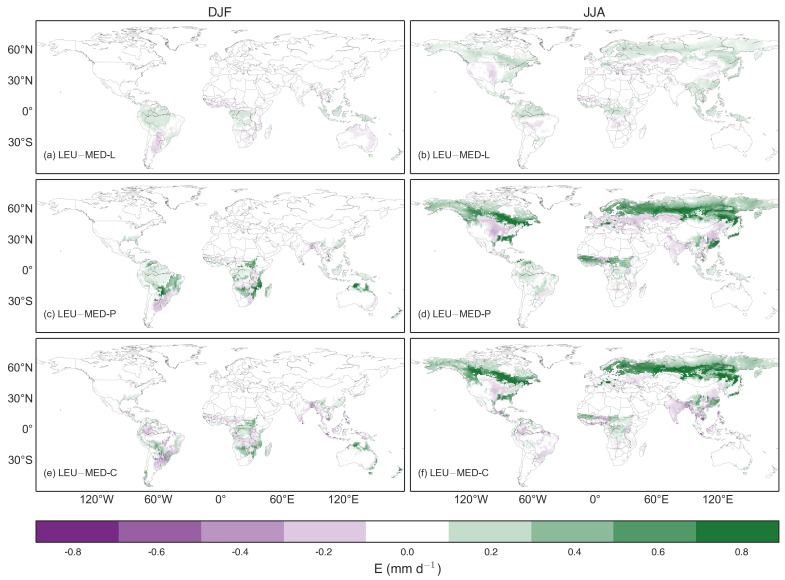

Figure 7. Mean seasonal (December-January-February: DJF and June-July-August: JJA) difference maps of transpiration (E) calculated across the 10 years of the Global Soil Wetness Project2 (GSWP2) forcing (1986–1995) period. **(a)** and **(b)** show the difference between the standard CABLE (LEU) model and the Medlyn model fit to the Leuning model (MED-L), **(c)** and **(d)** show the difference between the LEU model and the Medlyn model with the g_1 PFT parameterisation (MED-P), and finally, **(e)** and **(f)** show the difference between the LEU model and the Medlyn model with the g_1 parameter predicted as a function of climate indices (MED-C). In total, 126 pixels have been masked from **(e)** and **(f)**, representing pixels where the temperature range and moisture index extended outside the range of the synthesis g_s database. Data shown in **(c–f)** have been clipped, with the maximum ranges extending to (−0.3–1.12), (−0.33–1.27), (−0.63–0.84) and (−0.64–1.31) and this affects 36, 251, 8 and 444 pixels, respectively.

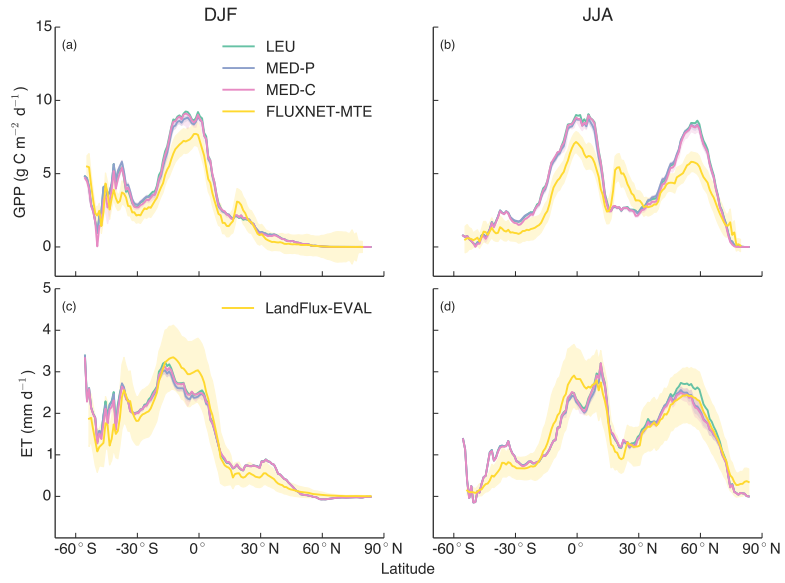

Figure 8. Latitudinal average (December-January-February: DJF and June-July-August: JJA) of mean annual **(a, b)** gross primary productivity (GPP) and **(c, d)** evapotranspiration (ET) predicted by the CABLE model compared to the upscaled FLUXNET and LandFlux-EVAL products. CABLE model predictions shown are from the standard CABLE (LEU), the Medlyn model fit to the Leuning model (MED-L), Medlyn model with the g_1 PFT parameterisation (MED-P) and the Medlyn model with the g_1 parameter predicted as a function of climate indices (MED-C). The shading represents ±1 SD in the data product and ±2 standard errors in the MED-P and MED-C models. Data shown cover the 10 years of the Global Soil Wetness Project2 (GSWP2) forcing (1986–1995) period. In total, 126 pixels have been masked from the zonal average of the MED-C model, which represents pixels where the temperature range and moisture index extended outside the range of the synthesis g_s database.

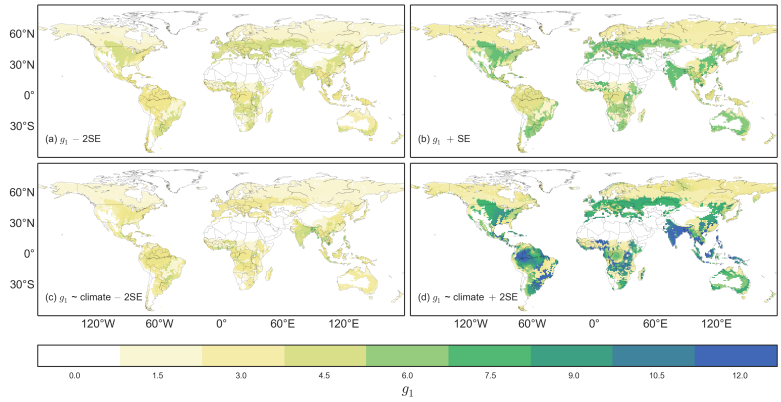

Figure A1. Global maps showing how the uncertainty of the g_1 model parameter. **(a)** shows −2 standard errors (SE) and **(b)** +2 SE for the fitted g_1 for each of CABLE's PFTs. **(c)** shows −2 standard errors (SE) and **(e)** +2 SE for predicted g_1 parameter values considering the influence of climate indices. In total, 126 pixels have been masked from **(c)** and **(d)**, representing pixels where the temperature range and moisture index extended outside the range of the synthesis g_s database.